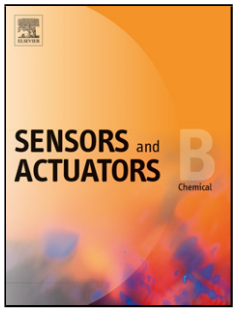


Title: Fabrication and Characterization of an Ultrasensitive Humidity Sensor Based on Metal Oxide/Graphene Hybrid Nanocomposite

Author: Dongzhi Zhang Hongyan Chang Peng Li Runhua Liu Qingzhong Xue

PII: S0925-4005(15)30606-7
DOI: http://dx.doi.org/doi:10.1016/j.snb.2015.11.024
Reference: SNB 19282

To appear in: *Sensors and Actuators B*

Received date: 11-5-2015
Revised date: 12-10-2015
Accepted date: 4-11-2015

Please cite this article as: D. Zhang, H. Chang, P. Li, R. Liu, Q. Xue, Fabrication and Characterization of an Ultrasensitive Humidity Sensor Based on Metal Oxide/Graphene Hybrid Nanocomposite, *Sensors and Actuators B: Chemical* (2015), http://dx.doi.org/10.1016/j.snb.2015.11.024

# Fabrication and Characterization of an Ultrasensitive Humidity Sensor Based on Metal Oxide/Graphene Hybrid Nanocomposite

**Dongzhi Zhang[1]*, Hongyan Chang[1], Peng Li[2], Runhua Liu[1], Qingzhong Xue[3]**

[1]College of Information and Control Engineering, China University of Petroleum (East China), Qingdao 266580, China

[2]State Key Laboratory of Precision Measurement Technology and Instruments, Department of Precision Instruments, Tsinghua University, Beijing 100084, China

[3]State Key Laboratory of Heavy Oil Processing, China University of Petroleum (East China), Qingdao 266580, PR China

*Corresponding author: Dongzhi Zhang

E-mail address: dzzhang@upc.edu.cn

Tel: +86-532-86981813 ext 426

Fax: +86-532-86981335





Page 1 of 39

**Abstract**

This paper demonstrated a flexible humidity sensor based on tin dioxide/reduced graphene oxide (RGO) nanocomposite film. The humidity sensor was fabricated on a polyimide substrate with microelectrodes by using a facile one-step hydrothermal route. The hydrothermal synthesized $SnO_2$ nanoparticles and $SnO_2$/RGO hybrid nanostructures were characterized by scanning electron microscopy (SEM) and X-ray diffraction (XRD). The humidity sensing properties of the presented $SnO_2$/RGO nano-hybrid sensor were investigated by exposing it to a broad humidity range of 11-97% RH at room temperature. Compared with traditional humidity sensors, the $SnO_2$ modified graphene sensor demonstrated an ultrahigh sensitivity and a rapid response/recovery characteristic over a full humidity range measurement, highlighting the unique advantages of hydrothermal synthesis for sensors fabrication. Finally, the possible humidity sensing mechanism of the proposed sensor was discussed by using complex impedance spectra and bode diagrams. These observed results demonstrate that RGO modified with metal oxide is promising nanomaterials for constructing high performance humidity sensors in widespread applications.

***Keywords***: tin oxide; reduced-graphene oxide; hydrothermal; humidity sensor





Page 2 of 39

## 1. Introduction

As a common type of sensor, humidity sensor is of vital importance in various applications for many aspects, such as industrial, medical, ecological and environmental monitoring [1, 2]. So far, various transduction techniques such as capacitive [3, 4], resistive [5, 6], optical fiber [7, 8], field effect transistor (FET) [9], surface acoustic wave (SAW) [10, 11], and quartz crystal microbalance (QCM) [12,13] have been used to fabricate humidity sensors. Moreover, several kinds of sensing materials including polymers [14], ceramics [15], metal oxide semiconductors (MOs) [16], carbon nanotubes and their composites [17] have been employed in humidity sensors. MOs-based humidity sensors exhibited certain advantages of low cost, simple construction, small size and compatibility with modern electronic devices, compared with other types of humidity sensors. Among them, tin dioxide ($SnO_2$) as a stable n-type semiconducting material with bandgap of 3.6eV, is one of popular candidates for making low-cost gas sensing devices, due to its unique physicochemical properties depend upon the humidity surrounding them. However, $SnO_2$-based sensors commonly have the shortcoming of poor selectivity between gas species [18-19]. Parthibavarman *et al.* have synthesized $SnO_2$ nanoparticles by microwave irradiation method and investigated their humidity sensing properties in environment monitoring [18]. Yadav *et al.* have fabricated nanocrystalline $SnO_2$ thick film-based humidity sensor on alumina substrate using screen printing technique [19]. The pristine $SnO_2$ sensors exhibited certain advantages when compared to other types of humidity sensors, but do not have abruptly change the resistance values at higher RH due to its



Page 3 of 39

high resistivity, limiting their commercialization and practical applications. Researchers have reported in improving the humidity sensitivity of $SnO_2$ by element doping, such as $La^{3+}$, $Ce^{3+}$, $K^+$ and $Sb^{3+}$ [20-22]. However, either the high cost or the less availability of many of these dopants is a disadvantage to use them.

Currently, graphene has attracted significant interest for a wide range of applications as an excellent nanomaterial, which is mainly attributed to its large specific surface area of 2600 $m^2$ $g^{-1}$, high chemical stability, and exceptional electrical properties such as low noise level and high carrier mobility [23]. Many efficient sensors based on graphene and its derivatives have been constructed for the detection of environmental gases, such as $H_2$, $NO_2$, $NH_3$, acetone and acetylene [24-28]. Among graphene derivatives, graphene or reduced graphene oxide (RGO) has aroused tremendous attentions currently due to its facile preparation and novel applications [29-30]. Notably, recent advances demonstrated that the decoration of graphene with metal oxide nanoparticles was an effective method for constructing high-performance sensors [31]. RGO as highly conductive $sp^2$ carbon atom film, serving as an anchor to promote the electrons transfer in the metal oxide nanoparticles, thus lead to a better sensing performance. Liu *et al.* constructed $NO_2$ gas sensor using RGO-ZnO hybrid composite as sensing material [32]. Wang *et al.* fabricated an efficient gas sensor based on CuO-ZnO/RGO ternary composite, exhibiting more outstanding sensing properties to acetone than that of CuO-ZnO and ZnO/RGO, respectively [33]. Esfandiar *et al.* successfully synthesized ribbon-like Pd-$WO_3$ incorporated RGO nanostructure as efficient hydrogen gas sensor [34]. These investigations



Page 4 of 39

demonstrated that the graphene-based metal oxide nanocomposite exhibited a large enhancement in gas sensing properties in comparison with pure metal oxide or graphene counterpart.

The aim of this work is to investigate a flexible capacitive humidity sensor based on $SnO_2$ decorated RGO nano-hybrid film for realizing high-performance at room temperature, which was successfully prepared by using a facile method of one-step hydrothermal treatment. The structure of RGO/$SnO_2$ hybrid composite was characterized by SEM and XRD. The humidity sensing behavior of the as-prepared RGO/$SnO_2$ hybrid composite was investigated under various relative humidity (RH) levels. This humidity sensor exhibited an ultrahigh sensitivity and a short response/recovery time over a wide range of RH levels. Furthermore, the possible humidity sensing mechanism of the proposed sensor was discussed by using complex impedance spectra and bode diagrams.

## 2. Experiment

### *2.1 Materials*

Tin tetrachloride pentahydrate ($SnCl_4 \cdot 5H_2O$) (≥99%) was offered by Shanghai Hansi Chemical Industry Co. Ltd (Shanghai, China). The graphene oxide (GO) nanosheets (>99%) were supplied by Chengdu Organic Chemicals Co. Ltd. All the above chemicals were used as received without further treatment.

### *2.2 Sensor fabrication*

The sensor was fabricated on a flexible polyimide (PI) substrate through microfabrication technology. The polyimide here is only used as substrate, and the



Page 5 of 39

electrodes are fabricated by metal sputtering. Fig.1 (a) shows the illustration of microfabrication process for the sensor. A 20 μm thick Cu/Ni layer was firstly deposited on PI substrate (75 μm thick) with a sputtering system. Subsequently, photoresist (PR) was applied to make a pair of interdigital electrodes (IDEs) pattern by using lithography technique, and then the redundant Cu/Ni was etched out to form micro-IDEs by using exposure and development. A sensing film was finally coated on the sensor surface. The IDEs pattern window on the PI substrate provided an outline dimension of 5×5 mm, the IDE finger thickness was 20 μm, and the width and gap both was 75 μm. Fig. 1 (b) shows the optical image of 4×6 sensors array on a flexible PI substrate.

The sensing film of $SnO_2$/RGO hybrid composite was prepared by using a facile route of hydrothermal treatment of $SnCl_4$ solution in the presence of graphene oxide. Firstly, 2 mL of GO (0.5 mg/mL) and 24 mg of $SnCl_4 \cdot 5H_2O$ were added into 20 mL of DI water by sonication for 10 min (40 kHz) and stirring for 1 h. Followed by transferring the above resulting solution into a 40 mL Teflon-lined, stainless-steel autoclave and heated at 180 ℃ for 12 h. GO was converted into conductive RGO under hydrothermal reduction. After the autoclave was cooled down to room temperature, the as-prepared products were obtained via centrifugation at 3000 r/min for 10 min, subsequent washing with DI water for several times to remove excess chloride ion. Finally, the resulting $SnO_2$/RGO dispersion was drop-casted onto the substrate, and followed by vacuum-drying in an oven at 50 ºC for 2 h. Moreover, RGO film was prepared for purpose of subsequent characterization by the above



Page 6 of 39

method but without addition of $SnCl_4 \cdot 5H_2O$.

*2.3 Instrument and analysis*

The surface morphologies of RGO and $SnO_2$/RGO hybrid composite were inspected with field emission scanning electron microscopy (FESEM, Hitachi S-4800, Japan). The XRD pattern for RGO and $SnO_2$/RGO were characterized with an X-ray diffractometer (Rigaku D/Max 2500PC, Japan) using Cu Kα (λ=1.5418 Å) radiation, a scanning range of diffraction angle (2θ) was 10-80°, and a scanning rate was 2°/min.

The experimental setup used for humidity sensing measurement is described in our previous work [6]. The experiments were performed at an ambient temperature of 25 ºC. The humidity sensing properties were investigated by exposing the $SnO_2$/RGO hybrid composite sensor to various relative humidity (RH) levels, which were achieved by several saturated aqueous solutions. Saturated solutions of LiCl, $CH_3COOK$, $MgCl_2$, $K_2CO_3$, $Mg(NO_3)_2$, $CuCl_2$, NaCl, KCl and $K_2SO_4$ in a closed vessel were employed to obtain 11%, 23%, 33%, 43%, 52%, 67%, 75%, 85% and 97%RH levels, respectively. The electrical properties of the proposed sensor prototype under various RH levels were measured by using a precision LCR meter (TH2828, China). The response of the sensor as a function of RH was achieved by exposing it inside the closed vessels with different RH levels (11-97%) for the adsorption of water molecules, and the sensor could be recovered upon exposure to dry air conditioned by phosphorus pentoxide ($P_2O_5$) powder (RH 0%) for the release of water molecules. Sensitivity (S) used to characterize the sensor performance was defined as $S=\Delta C/\Delta RH$ (Unit: pF/%RH), where $\Delta C$ is the sensor response change in



Page 7 of 39

capacitance, and ΔRH is the RH change. The hysteresis error was defined as a deviation due to hysteresis between upscale-going and downscale-going indications in terms of the full measured quantity. The time taken by a sensor to achieve 90% of the total resistance change is defined as the response or recovery time.

## 3. Results and discussion

### *3.1 SEM and XRD characterization*

Fig. 2 shows the observed SEM images of as-prepared RGO film and $SnO_2$/RGO hybrid composite. The SEM image of RGO in Fig. 2(a) indicates that the RGO film has wrinkles which overlap at the edges, and exhibit randomly aggregated RGO sheets. Fig.2 (b) exhibits the nanosphere-shaped $SnO_2$ nanocrystals, and Fig. 2(c) shows that $SnO_2$ nanocrystals are attached on the surface of RGO sheets, in which the presence of $SnO_2$ nanocrystals reveals that hydrothermal treatment of GO and $SnCl_4$ solution is an effective method for synthesizing $SnO_2$/RGO hybrid composite.

The XRD characterization for RGO, $SnO_2$ and $SnO_2$/RGO hybrid composite is illustrated in Fig. 3. The XRD pattern of RGO in Fig. 3 (a) shows a prominent peak at $2\theta$ angle of 24.7°, which is attributed to RGO, in contrast with the data in the diffraction standard for RGO (PDF#74-2330 RIR 10.41). According to the Bragg formula, $\lambda=2d\sin(\theta)$, the interlayer distance $d$ of the RGO can be determined as 3.60 Å ($2\theta$ = 24.7°). The XRD spectrum of $SnO_2$ in Fig. 3 (b) exhibits several strong scatting peaks at 2θ of 26.41, 33.82, 37.60, 51.73 and 65.68°, which were attributed to the (1 1 0), (1 0 1), (2 0 0), (2 1 1) and (3 0 1) planes of $SnO_2$ nanocrystals (JCPDS Card no. 41-1445). The crystallite size can be estimated by using Debye-Scherer



Page 8 of 39

formula, $D=K\lambda/(\beta\cos\theta)$. Here $\beta$ is the full width at half maximum of the peak, and K=0.94 is a dimensionless constant. The highest intensity peak, centred at $2\theta$=26.41°, was assigned to $SnO_2$ (1 1 0) reflection having d-spacing of 3.37 Å and crystallite size as 3.25 nm. It is visible that the broad peak for RGO is not obvious in the XRD pattern of $SnO_2$/RGO hybrid composite shown in Fig. 3 (c), probably due to that the RGO is wrapped by $SnO_2$ nanocrystals through the hydrothermal treatment, or the weak peak of RGO is swamped by the presence of the strong peak around 26.41° at (1 1 0) plane of the $SnO_2$ nanocrystals.

*3.2 Humidity-sensing properties*

Fig.4 plots the capacitance of the $SnO_2$/RGO hybrid composite sensor versus RH at different working frequencies of 10, 40, 70 and 100 kHz. It is found that the sensor capacitance dependent on RH at different working frequencies. As the RH level increases, the sensor capacitance shifts higher monotonically. This can be interpreted as that, the absorbed water molecules are beneficial to strengthen the polarization effect and increase the dielectric constant, lead to an increase of sensor capacitance with rising RH [35-36]. Among the four frequencies, the sensor at 10 kHz exhibits the highest capacitance response as well as the highest sensitivity. And thus, 10 kHz was selected as the working frequency in the following experiments. In order to investigate the effect of different loading of $SnO_2$ toward RH detection, several sensor samples with different loading of $SnO_2$ were examined under exposure of 75%RH. The inset in Fig.4 shows the influence of the $SnCl_4 \cdot 5H_2O$ amount (12, 24, 36 and 48 mg) on the sensor sensitivity. The sensor sensitivity was increased and reaches a



Page 9 of 39

maximum value for the sample with the amount of $SnCl_4$ at 24 mg, and then decreases with further increasing the amount to 48 mg. This could be explained by the fact that the increased amount of $SnO_2$ result in film aggregation, which leads to a decreased in sensor sensitivity. Therefore, the optimized amount of 24 mg $SnCl_4 \cdot 5H_2O$ was used to prepare sensor samples.

Fig. 5 illustrates that the capacitance response at 10 kHz for the sensor upon exposure to different RH levels. The reversibility and reproducibility of the sensor was examined through exposure/recovery cycles for the sensor exposed from low RH to high RH, and then conversely from high RH to low RH. Each exposure/recovery cycle was performed by an exposure interval of 100 s to a given RH, and followed by a recovery interval of 100 s at dry air. As noted in Fig.6, the sensor exhibited a great change in capacitance from 246.53 pF to 138267 pF over the humidity range from 11% to 97%RH, and an ultrahigh sensitivity was calculated to be 1568.42pF/%RH. The corresponding capacitance changes by approximately 550-folds of magnitude within the entire humidity range of 11-97%RH.

In the above measurements, the RH exposure interval was chosen to be 100 s in order to demonstrate the potential of the prepared sensor in the application of real-time RH monitoring, where an immediate response to varying RH is necessary. However, it is equally important to consider the response and recovery times of our sensors to given RH environment. Adequate exposure time is performed for reaching equilibrium stage. Fig. 6 demonstrates the time-dependent response and recovery curves of the sensor to RH pulse between 0% and 23%, 43%, 67%, 97% RH,



Page 10 of 39

respectively. Response time of less than 102 s and recovery time of several seconds are observed in the RH measurements. In order to further investigate the sensor stability, the noise measurement was determined from data collected at equilibrium stage, and noise was determined from the standard deviation of the recorded capacitance. The noise level was 0.207, 3.45, 4.12 and 5.43 pF at 23%, 43%, 67%, 97% RH, respectively, which was much smaller than the other humidity sensors [37-39].

Fig.7 shows the sensitivity comparison between $SnO_2$/RGO composite and RGO toward humidity sensing. We can find that the sensitivity of the $SnO_2$/RGO composite is considerably higher than that of pure RGO, indicating the advantage of $SnO_2$/RGO composite for humidity sensing. The error bars represent standard deviation (SD) from the mean based on five sensors exposed to given RH. A standard deviation within 1.5% was obtained, indicating a good sensor-to-sensor reproducibility. And the inset indicates the humidity hysteresis of the $SnO_2$/RGO humidity sensor, which is a physical phenomenon caused by the physical properties of the element material. The sensor hysteresis was measured by increasing RH from 11% to 97% and then returned the RH back to 11%. The $SnO_2$/RGO hybrid composite film exhibits a relatively small hysteresis loop for the humidification and desiccation processes, and the maximum hysteresis error of 1.8% was observed through the comparison of humidification and desiccation processes.

The impedance-frequency characteristics of the $SnO_2$/RGO hybrid film sensor at different RH levels were further investigated, and the measured results are shown in



Page 11 of 39

Fig. 8 The impedances of the $SnO_2$/RGO hybrid composite sensor upon exposure of various RH levels under different working frequency from 2500 kHz to 1 MHz were presented. The impedance of the sensor under certain working frequency decreased with the rising of RH, and the inset in Fig.9 indicates the sensor impedance under various RH levels at 10 kHz. Moreover, it is notably that the impedance of the sensor under certain RH decreased with the increasing of working frequency and became flatly at high frequencies, indicating the influence of working frequencies on impedance was weakened at high frequency.

The sensing properties for the proposed sensor are comparable to those of capacitive-type humidity sensors in previous works [40-48], which are presented in Table 1. The comparison highlights the excellent performance of $SnO_2$/RGO hybrid composite film as a candidate for constructing humidity sensors, with sensitivity of 1568.440 pF/%RH, is more than 7 times than that of the best one among conventional capacitive humidity sensors at 11-97%RH.

3.3 *Humidity-sensing mechanism*

The sensitivity of the $SnO_2$/RGO composite is considerably higher than that of pure RGO, as Fig. 7 shown. Several possible reasons may be attributed for this enhancement in sensitivity. In general, the ability of RGO to detect water molecules depends on its high surface-to-volume ratios and hydrophilic functional groups attached on its surface, such as hydroxyl and carboxyl groups. The incorporation of $SnO_2$ NPs into RGO sheets brings more active sites, such as vacancies and defects. Heterojunction may be created at the interface of the two nanomaterials, and



Page 12 of 39

contributes to the improvement in humidity sensing. Furthermore, RGO has low resistivity and high carrier mobility, serving as an anchor to promote the electrons transfer in the metal oxide nanoparticles, which plays a role in modification of $SnO_2$.

The complex impedance spectra (CIS) were used to further investigate the humidity sensing mechanism in this paper. The CIS of the sensor shown in Fig.9 were measured at different RH levels under the working frequency of 2500 Hz to 1 MHz. Re(Z) and -Im(Z) were the real and imaginary parts of the CIS, and some of the real and imaginary parts were magnified on the same plane to make the CIS comparison conveniently. It is notable that the complex impedance spectra appeared to be a semicircle at 11%-52% RH, which can be described by an equivalent circuit comprising a resistor and a capacitor connected in parallel as shown in Fig. 10(a). The observed semicircle is attributed to the intrinsic impedance of the $SnO_2$/RGO sensing film, as suggested by Thakur et al. [49, 50]. In this condition, the chemisorpted water molecule on the film surface is not continuous, and the ionic conduction is difficult. The conductivity of the sensor at this stage is mainly due to the intrinsic charge carriers of $SnO_2$/RGO hybrid nanocomposite rather than the adsorbed water molecules.

As the RH increased to surpass 67% RH, much more water molecules were adsorbed and several water layers were formed, and the CIS exhibited the semicircle became smaller as RH increases and a short straight line appeared at the tail of the semicircle at low frequency range. This phenomenon reflects the contribution of the $SnO_2$/RGO film to the conduction become smaller and the adsorbed water become



Page 13 of 39

dominant. In this condition, more and more water molecules are trapped between the electrodes and the $SnO_2$/RGO film, resting in a strong diffusion behavior. The straight line at the tail of the semicircle was attributed to the diffusion process of ions or charge carriers at the sensing material/electrode interface [13]. The physisorbed water layers exhibit a liquid-like behavior, and $H_3O^+$ ions and $H^+$ hopping occurs in the charge transport by a Grotthuss chain reaction, $H_2O+H_3O^+ \leftrightarrow H_3O^+ + H_2O$ [51]. The equivalent circuit shown in Fig. 10 (b) is depicted by the series and parallel combinations of resistance, capacitor and Warburg impedance. Herein, the Warburg impedance ($Z_W$) was introduced to represent the short line [52]. The freely transfer of ions on the water layer resulted in a decrease in the impedance of the sensor impedance.

The parameters of EC model shown in Fig. 10 can be obtained by best fit of the impedance spectra data using the software Zview 3.3. The experimental data are indicated as dots, and the fits are represented as continuous lines. Fig.11 (a) plots the bode diagram for the EC model under the condition of 33% RH. The plot of log|Z| was little changed at low log *f* but decreased sharply at high log *f*, and the phase angle increased with the increasing frequency and approach to -90º at high frequency range. This is a typical characteristic of circuit with a resistor and a capacitor connected in parallel. Fig.11 (b) shows the bode diagram for the EC model under the condition of 97% RH. The phase angle increased with the increasing of working frequency but was far less than -90º at high frequency range. At high RH, the serial water layers further accelerated the transfer of electrons. The water molecules permeated into the



Page 14 of 39

mesopores of $SnO_2$/RGO film and electrolytic conduction occurred at this stage, and resulted in the impedance decreased dramatically.

## 4. Conclusions

This paper demonstrated a capacitive-type humidity sensor based on $SnO_2$/RGO nanocomposite film. The humidity sensor was fabricated on a polyimide substrate with microelectrodes by using a facile hydrothermal route. The hydrothermal synthesized $SnO_2$ nanoparticles and $SnO_2$/RGO nanostructures were characterized by scanning electron microscopy (SEM) and X-ray diffraction (XRD). The humidity sensing properties of the presented $SnO_2$/RGO nano-hybrid sensor were investigated by exposing it to a broad humidity range of 11-97% RH at room temperature. Compared with traditional humidity sensors, the $SnO_2$ modified graphene sensor demonstrated an ultrahigh sensitivity and a fast response/recovery characteristic over a full humidity range measurement, highlighting the unique advantages of hydrothermal synthesis for sensors fabrication. The possible sensing mechanism for the sensor was proposed and discussed by using complex impedance spectra and bode diagrams.



## Acknowledgements

This work was supported by the National Natural Science Foundation of China (Grant no. 51407200, and 51405257), the Science and Technology Development Plan Project of Shandong Province of China (Grant no. 2014GSF117035), the Promotive



Page 15 of 39

Research Foundation for the Excellent Middle-Aged and Youth Scientists of Shandong Province of China (Grant no. BS2012DX044), the Science and Technology Development Plan Project of Qingdao (Grant no. 13-1-4-179-jch), the Open Fund of National Engineering Laboratory for Ultra High Voltage Engineering Technology (Kunming, Guangzhou) (Grant no. NEL201518), the Fundamental Research Funds for the Central Universities of China (Grant no. 15CX05041A), and the Science and Technology Project of Huangdao Zone, Qingdao, China (Grant no. 2014-1-51).





Page 16 of 39

**References**

[1] T. Yang, Y.Z. Yu, L.S. Zhu, X. Wu, X.H. Wang, J. Zhang, Fabrication of silver interdigitated electrodes on polyimide films via surface modification and ion-exchange technique and its flexible humidity sensor application, Sens. Actuators B 208 (2015) 327-333.

[2] P.-G. Su, C.-F. Chiou, Electrical and humidity-sensing properties of reduced graphene oxide thin film fabricated by layer-by-layer with covalent anchoring on flexible substrate, Sens. Actuators B 200 (2014) 9-18.

[3] A. Rivadeneyra, J. F.-Salmerón, M. Agudo, J. A. L.-Villanueva, L.F. C.-Vallvey, A.J. Palma, Design and characterization of a low thermal drift capacitive humidity sensor by inkjet-printing, Sens. Actuators B 195 (2014) 123-131.

[4] D.Z. Zhang, J. Tong, B.K. Xia, Q.Z. Xue, Ultrahigh performance humidity sensor based on layer-by-layer self-assembly of graphene oxide/polyelectrolyte nanocomposite film, Sens. Actuators B 203 (2014) 263-270.

[5] P. Cavallo, D.F. Acevedo, M.C. Fuertes, G. J.A.A. Soler-Illia, C.A. Barbero, Understanding the sensing mechanism of polyaniline resistive sensors. Effect of humidity on sensing of organic volatiles, Sens. Actuators B, 210 (2015) 574-580.

[6] D.Z. Zhang, J. Tong, B.K. Xia, Humidity-sensing properties of chemically reduced graphene oxide/polymer nanocomposite film sensor based on layer-by-layer nano self-assembly, Sens. Actuators B 197 (2014) 66-72.

[7] M. Batumalay, S.W. Harun, N. Irawati, H. Ahmad, H. Arof, A study of relative humidity fiber-optic sensors, IEEE Sens. J. 15 (2015) 1945-1950.



Page 17 of 39

[8] H. Sun, X. Zhang, L. Yuan, L. Zhou, X. Qiao, M. Hu, An optical fiber fabry-perot interferometer sensor for simultaneous measurement of relative humidity and temperature, IEEE Sens. J. 15 (2015) 2891-2897.

[9] C. Sun, K.R.G. Karthik, S.S. Pramana, L.H. Wong, J. Zhang, H. Yizhong, C.H. Sow, N. Mathews, S.G. Mhaisalkar, The role of tin oxide surface defects in determining nanonet FET response to humidity and photoexcitation, J. Mater. Chem. C 2 (2014) 940-945.

[10] H.S. Hong, G.S. Chung, Controllable growth of oriented ZnO nanorods using Ga-doped seed layers and surface acoustic wave humidity sensor, Sens. Actuators B 195 (2014) 446-451.

[11]Y. Tang, Z. Li, J. Ma, L. Wang, J. Yang, B. Du, Q. Yu, X. Zu, Highly sensitive surface acoustic wave (SAW) humidity sensors based on sol-gel $SiO_2$ films: Investigations on the sensing property and mechanism, Sens. Actuators B 215 (2015) 283-291.

[12] Y. Yao, Y. Xue, Impedance analysis of quartz crystal microbalance humidity sensors based on nanodiamond/graphene oxide nanocomposite film, Sens. Actuators B 211 (2015) 52-58.

[13] Y. Zhu, J. Chen, H. Li, Y. Zhu, J. Xu, Synthesis of mesoporous $SnO_2$-$SiO_2$ composites and their application as quartz crystal microbalance humidity sensor, Sens. Actuators B 193 (2014) 320-325.

[14] T. Fei, K. Jiang, S. Liu, T. Zhang, Humidity sensor based on a cross-linked porous polymer with unexpectedly good properties, RSC Adv. 4 (2014)



Page 18 of 39

21429-21434.

[15] T. Nenov, Z. Nenova, Multi-objective optimization of the parameters of $TiO_2$-based ceramic humidity sensors, Ceram. Int. 39 (2013) 4465-4473.

[16] S. G. Chatterjee, S.Chatterjee, A.K. Ray, A.K. Chakraborty, Graphene-metal oxide nanohybrids for toxic gas sensor: A review, Sens. Actuators B 221(2015) 1170-1181.

[17] T. Fei, K. Jiang, F. Jiang, R. Mu, T. Zhang, Humidity switching properties of sensors based on multiwalled carbon nanotubes/polyvinyl alcohol composite films, J. Appl. Polym. Sci. 131 (2014) 39726.

[18]M. Parthibavarman, V, Hariharan, C. Sekar, High-sensitivity humidity sensor based on $SnO_2$ nanoparticles synthesized by microwave irradiation method, Mater. Sci. Eng. C 31 (2011) 840-844.

[19]B.C. Yadav, R. Singh, S. Singh, Investigations on humidity sensing of nanostructured tin oxide synthesised via mechanochemical method, J. Exp. Nanosci. 8 (2013) 670-683.

[20]H. Li, Z. Shi, H. Liu, Humidity sensing properties of $La^{3+}$/$Ce^{3+}$-doped $TiO_2$-20 wt.% $SnO_2$ thin films derived from sol-gel method, J. Rare Earth 28 (2010)123-127.

[21]X. Song, Q. Qi, T. Zhang, C. Wang, A humidity sensor based on KCl-doped $SnO_2$ nanofibers, Sens. Actuators B 38 (2009) 368-373.

[22]J. Huang, J. Wang, A.A. Zhukova, M.N. Rumyantseva, A.M. Gaskov, K.Yu, C. Gu, J. Liu, High-sensitivity humidity sensor based on a single Sb-doped $SnO_2$



Page 19 of 39

whisker, Sens. Lett. 7 (2009) 1025-1029.

[23] O.C. Compto, S.T. Nguyen, Graphene oxide, highly reduced graphene oxide, and graphene: versatile building blocks for carbon-based materials, Small 6 (2010) 711-723.

[24] J. Hong, S. Lee, J. Seo, S. Pyo, J. Kim,T. Lee, A highly sensitive hydrogen sensor with gas selectivity using a PMMA membrane-coated Pd nanoparticle/ single-layer graphene hybrid, ACS Appl. Mater. Interfaces, 7 (2015) 3554-3561.

[25] H. Zhang, J.C. Feng, T. Fei, S. Liu, T. Zhang, $SnO_2$ nanoparticles-reduced graphene oxide nanocomposites for $NO_2$ sensing at low operating temperature, Sens. Actuators B 190 (2014) 472-478.

[26] N. Hu, Z. Yang, Y. Wang, L. Zhang, Y. Wang, X. Huang, H. Wei, L. Wei, Y. Zhang, Ultrafast and sensitive room temperature $NH_3$ gas sensors based on chemically reduced graphene oxide, Nanotechnology 25 (2014) 025502.

[27] D. Zhang, A. Liu, H. Chang, B. Xia, Room-temperature high-performance acetone gas sensor based on hydrothermal synthesized $SnO_2$-reduced graphene oxide hybrid composite, RSC Adv. 5 (2015) 3016-3022.

[28] A.S.M.I. Uddin, D.T. Phan, G.S. Chung, Low temperature acetylene gas sensor based on Ag nanoparticles-loaded ZnO-reduced graphene oxide hybrid, Sens. Actuators B 207 (2015) 362-369.

[29] W.J. Yuan, G.Q. Shi, Graphene-based gas sensors, J. Mater. Chem. A 1 (2013)10078-10091.

[30] S.S. Varghese, S. Lonkar, K.K. Singh, S. Swaminathan, A. Abdala, Recent



Page 20 of 39

advances in graphene based gas sensors, Sens. Actuators B. 218 (2015) 160-183.

[31] Y. Yang, C. Tian, J. Wang, L. Sun, K. Shi, W. Zhou, H. Fu, Facile synthesis of novel 3D nanoflower-like CuxO/multilayer graphene composites for room temperature NOx gas sensor application, Nanoscale 6 (2014) 7369-7378.

[32] S. Liu, B. Yu, H. Zhang, T. Fei, T. Zhang, Enhancing $NO_2$ gas sensing performances at room temperature based on reduced graphene oxide-ZnO nanoparticles hybrids, Sens. Actuators B 202 (2014) 272-278.

[33] Z.Y. Wang, Y. Xiao, X.B. Cui, P.F. Cheng, B. Wang, Y. Gao, X.W. Li, T.L. Yang, T. Zhang, G.Y. Lu, Humidity-sensing properties of urchinlike CuO nanostructures modified by reduced graphene oxide, ACS Appl. Mater. Interfaces 6 (2014) 3888-3895.

[34] A. Esfandiar, A. Irajizad, O. Akhavan, S. Ghasemi, M.R. Gholami, Pd-$WO_3$/reduced graphene oxide hierarchical nanostructures as efficient hydrogen gas sensors, Int. J. Hydrogen Energy 39 (2014) 8169-8179.

[35] S. Pokhrel, K.S. Nagaraja, Electrical and humidity sensing properties of chromium (III) oxide-tungsten (VI) oxide composites, Sens. Actuators B 92 (2003) 144-150.

[36] B.H. Cheng, B.X. Tian, C.C. Xiao, Y.H. Xiao, S.J. Lei, Highly sensitive humidity sensor based on amorphous $Al_2O_3$ nanotubes, J. Mater. Chem. 21 (2011) 1907-1912.

[37] S. Lei, C. Deng, Y. Chen, Y. Li, A novel serial high frequency surface acoustic wave humidity sensor, Sens. Actuators A: Phys. (2011) 167, 231-236.



Page 21 of 39

[38] P. Pang, J. Guo, S. Wu, Q. Cai, Humidity effect on the dithiol-linked gold nanoparticles interfaced chemiresistor sensor for VOCs analysis, Sens. Actuators B: Chem. (2006) 114, 799-803.

[39]T. Li, X. Liu, C. Dong, L. Yin, Single chip integration of MWCNTs/$SiO_2$ thin film humidity sensor based on standard CMOS IC process, Microelectron. Eng. (2014)119, 155-158.

[40]H.C. Bi, K.B. Yin, X. Xie, J. Ji, S. Wan, L.T. Sun, M. Terrones, M.S. Dresselhaus, Ultrahigh humidity sensitivity of graphene oxide, Sci Rep. 3 (2013) 2714.

[41]V.P.J. Chung, M.C. Yip and W. Fang, Resorcinol-formaldehyde aerogels for CMOS-MEMS capacitive humidity sensor, Sens. Actuators B, 214 (2015) 181-188.

[42]M.Z. Yang, C.L. Daiand C.C. Wu, Sol-gel zinc oxide humidity sensors integrated with a ring oscillator circuit on-a-chip, Sensors 14(2014) 20360-20371.

[43]A. Arena, N. Donato, G. Saitta, Capacitive humidity sensors based on MWCNTs/ polyelectrolyte interfaces deposited on flexible substrates, Microelectron. J. 40 (2009) 887-890.

[44]B.R. Tao, J. Zhang, F.J. Miao, H.L. Li, L.J. Wan, Y.T. Wang, Capacitive humidity sensors based on Ni/SiNWs nanocomposites, Sens. Actuators B 136 (2009) 144-150.

[45]F.U. Rehman, M.Tahir, S. Hameed, F. Wahab, D.N. Khan, F. Aziz, F.A. Khalid, M.N. Khalid, W. Ali, Investigating sensing properties of poly-(dioctylfluorene) based planar sensor, Mater. Sci. Semicond. Process. 39 (2015) 355-361.



Page 22 of 39

[46] J.H. Kim, S.M. Hong, B.M. Moon, K. Kim, High-performance capacitive humidity sensor with novel electrode and polyimide layer based on MEMS technology, Microsyst. Technol. 16 (2010) 2017-2021.

[47] T. Islam, Md. R.Mahboob, A simple MOX vapor sensor on polyimide substrate for measuring humidity in ppm level, IEEE Sens. J. 5 (2015) 3004-3015.

[48] T. Yang, Y.Z. Yu, L.S. Zhu, X. Wu, X.H. Wang, J. Zhang, Fabrication of silver interdigitated electrodes on polyimide films via surface modification and ion-exchange technique and its flexible humidity sensor application, Sens. Actuators B 208 (2015) 327-333.

[49] S. Thakur, P. Patil, Rapid synthesis of cerium oxide nanoparticles with superior humidity-sensing performance, Sens. Actuators B. 194(2014) 260-268.

[50] Z.O. Uygun, H.D.E. Uygun, A short footnote: Circuit design for faradaic impedimetric sensors and biosensors, Sens. Actuators B. 202 (2014) 448-453.

[51]N. Agmon, The Grotthuss mechanism, Chem. Phys. Lett. 244 (1995) 456-462.

[52]K. Jiang, T. Fei, T. Zhang, Humidity sensor using a Li-loaded microporous organic polymer assembled by 1,3,5-trihydroxybenzene and terephthalic aldehyde, K. Jiang, T. Fei, T. Zhang, RSC Adv. 4 (2014) 28451-28455.





Page 23 of 39

**Table 1**

Performance of the presented sensor in this work compared with previous work.

| Sensing material | Fabrication method | Measurement range | Sensitivity | Ref. |
|---|---|---|---|---|
| RGO/$SnO_2$ | Hydrothermal synthesis | 11-97%RH | 1568.440pF/%RH | this paper |
| GO | Solution dripping | 15%-95%RH | 46.253pF/%RH | [40] |
| Resorcinol-formaldehyde | Sol-gel method | 18%-83%RH | 20 fF/%RH | [41] |
| ZnO | Sol-gel method | 40%-90%RH | 2.800 pF/%RH | [42] |
| MWCNTs/polyelectrolyte | Solution dripping | 35%-60%RH | 4.200 pF/%RH | [43] |
| Ni/SiNWs | Electroplating method | 11.3%-97.3%RH | 232.558pF/%RH | [44] |
| poly-(dioctylfluorene) | Solution dripping | 65%-80%RH | 6.400 pF/%RH | [45] |
| Polyimide | Spin-coating | 10%-90%RH | 506fF/%RH | [46] |
| polyimide -$Al_2O_3$ | Sol-gel method | 10%-98%RH | 4 pF/%RH | [47] |
| Polyimide | inkjet-printing method | 16%-90%RH | 43.919 pF/%RH | [48] |





Page 24 of 39

## List of figures

**Figure 1.** (a) Optical image of sensor array on a flexible PI substrate. (b) Schematic illustration of as-fabricated sensor prototype.

**Figure 2.** Typical SEM images of (a) RGO film, (b) $SnO_2$ nanoparticles and (c) $SnO_2$/RGO hybrid composite.

**Figure 3.** XRD spectra of RGO, $SnO_2$ and $SnO_2$/RGO hybrid composite.

**Figure 4.** Capacitance of $SnO_2$/RGO hybrid composite sensor versus RH at 10 kHz, 40 kHz, 70 kHz and 100 kHz. Inset: Sensitivity of the sensor samples with different loading of $SnO_2$ under exposure of 75%RH at 10 kHz.

**Figure 5.** Capacitance response of the $SnO_2$/RGO hybrid composite sensor under switching RH.

**Figure 6.** Response and recovery curves of the $SnO_2$/RGO hybrid composite sensor toward a RH pulse from dry air to other RH levels.

**Figure 7.** Sensitivity comparison between $SnO_2$/RGO composite and RGO toward humidity sensing. Inset: Hysteresis characteristic of the $SnO_2$/RGO composite humidity sensor.

**Figure 8.** Impedance-frequency characteristics of the $SnO_2$/RGO hybrid composite sensor at various RH levels, the inset indicates the sensor impedance under various RH levels at 10 kHz.

**Figure 9.** Complex impedance spectra of $SnO_2$/RGO film sensor at different relative humidity. ImZ: imaginary part; ReZ: real part.

**Figure 10.** Impedance-frequency characteristics of the $SnO_2$/RGO hybrid composite



Page 25 of 39

sensor at different RH levels. $R_f$: film resistance; $C_f$: film capacitance; $Z_W$: Warburg impedance.

**Figure 11.** Bode diagrams of $SnO_2$/RGO hybrid composite sensor at different RH: (a) 33%RH, (b) 97%RH.





Page 26 of 39

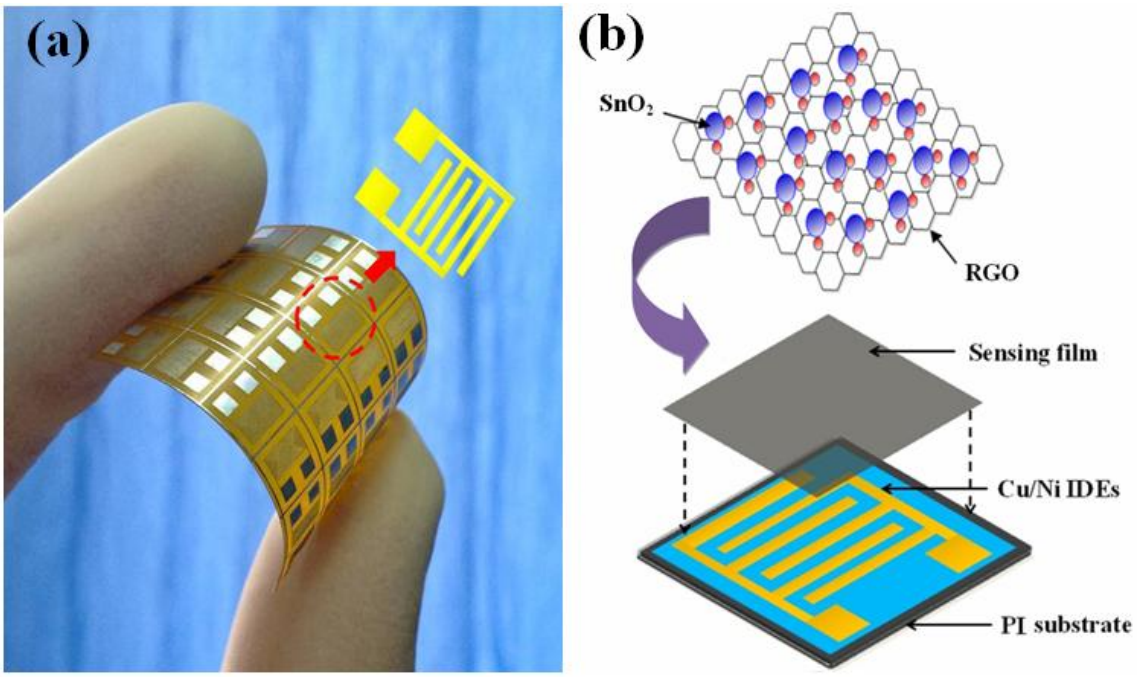


**Figure 1.** (a) Optical image of sensor array on a flexible PI substrate. (b) Schematic illustration of as-fabricated sensor prototype.





Page 27 of 39

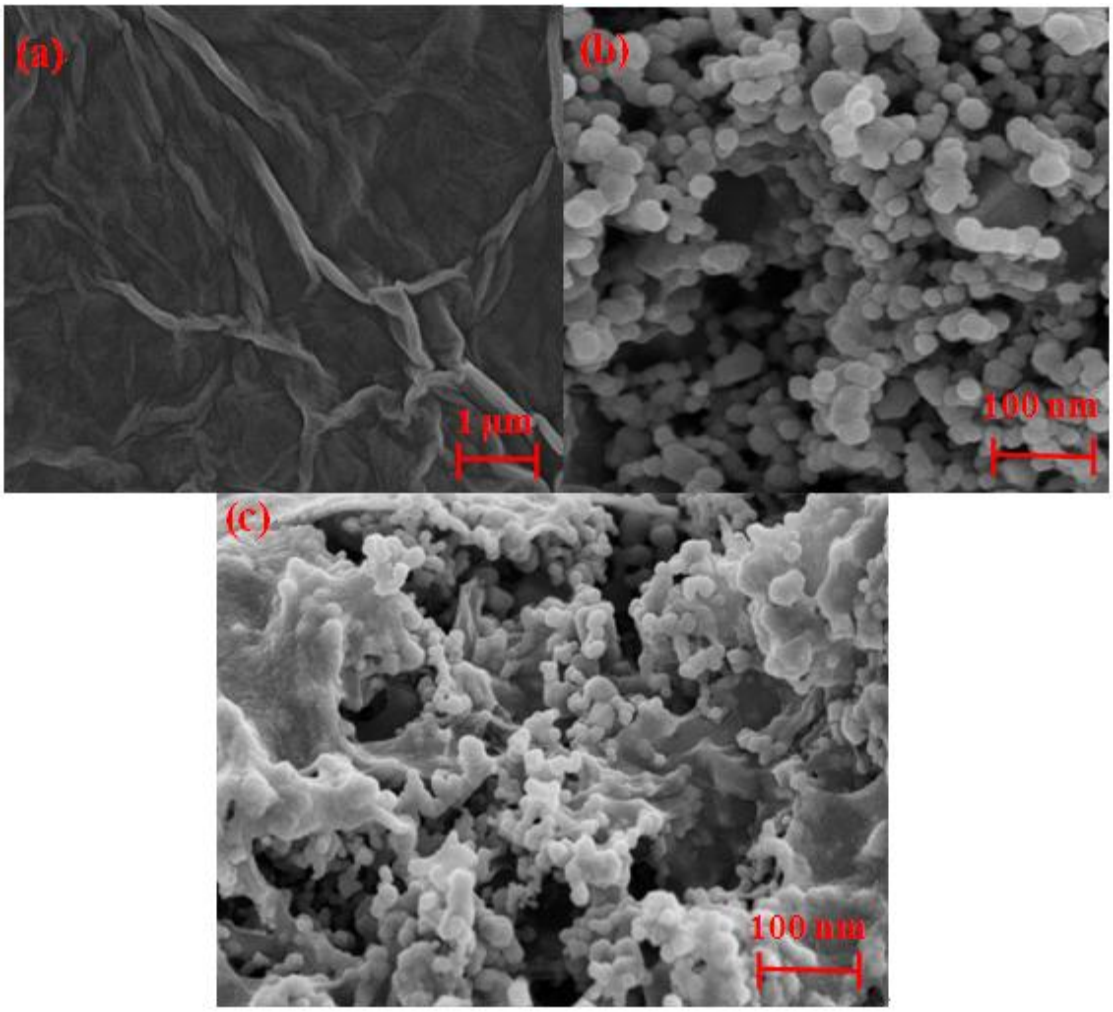


**Figure 2.** Typical SEM images of (a) RGO film, (b) $SnO_2$ nanoparticles and (c) $SnO_2$/RGO hybrid composite.





Page 28 of 39

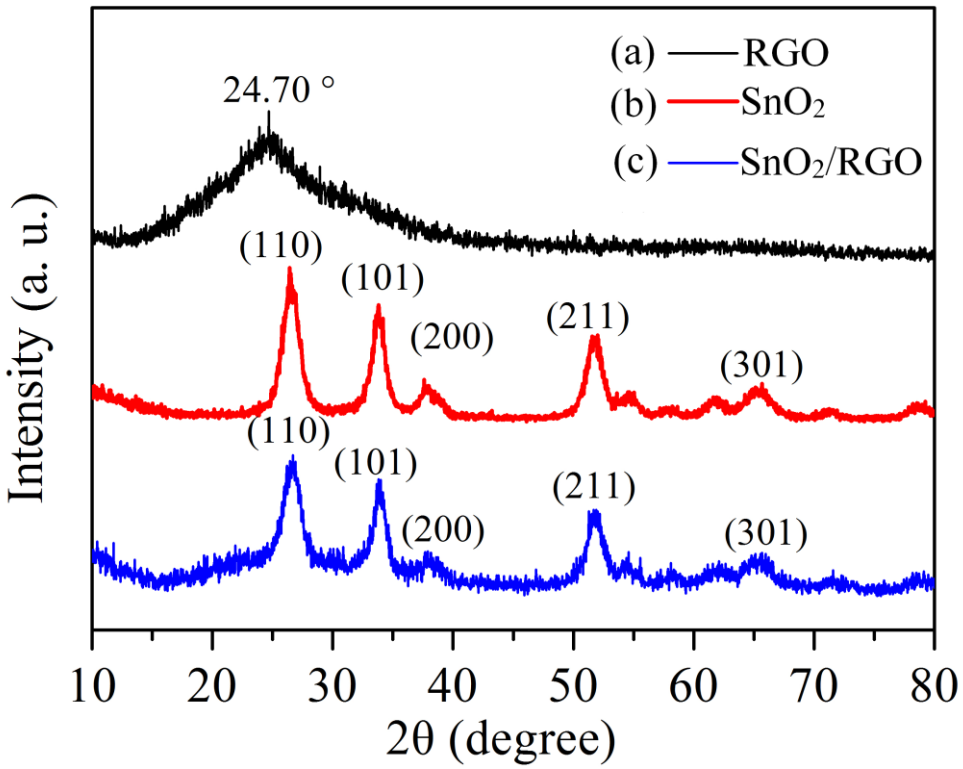


**Figure 3.** XRD spectra for RGO, $SnO_2$ and $SnO_2$/RGO hybrid composite.



Page 29 of 39

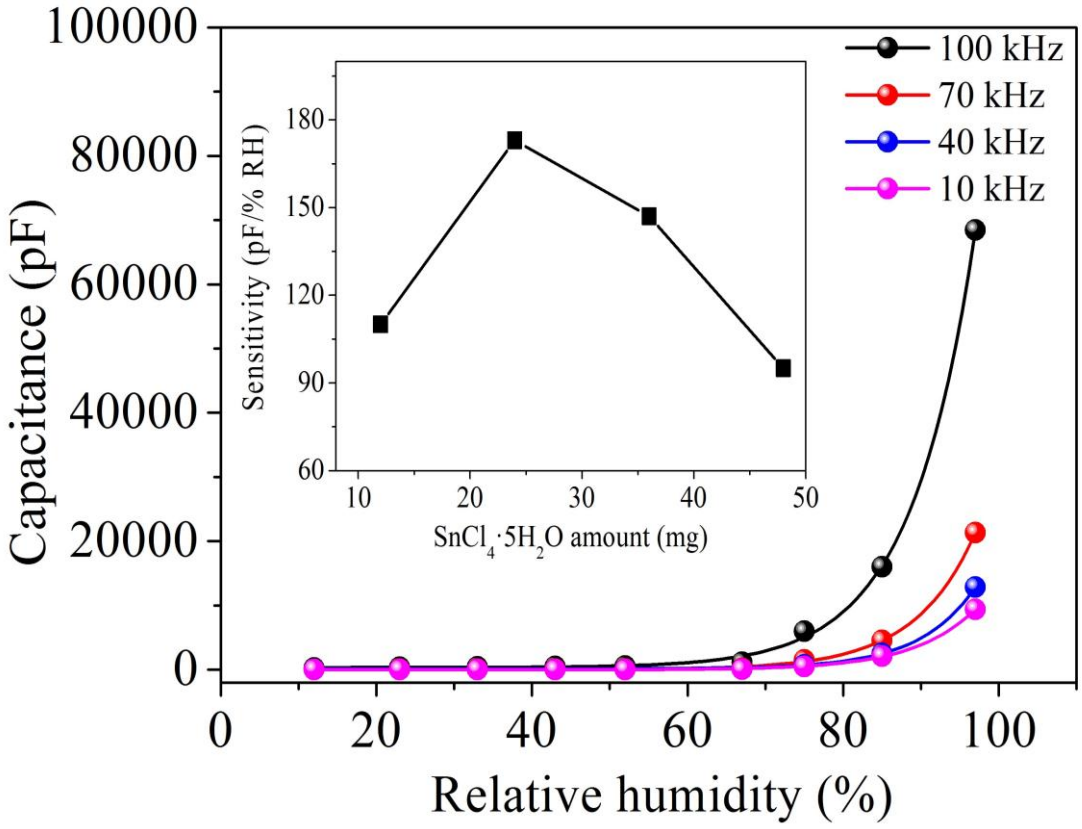


**Figure 4.** Capacitance of $SnO_2$/RGO hybrid composite sensor versus RH at 10 kHz, 40 kHz, 70 kHz and 100 kHz. Inset: Sensitivity of the sensor samples with different loading of $SnO_2$ under exposure of 75%RH at 10 kHz.



Page 30 of 39

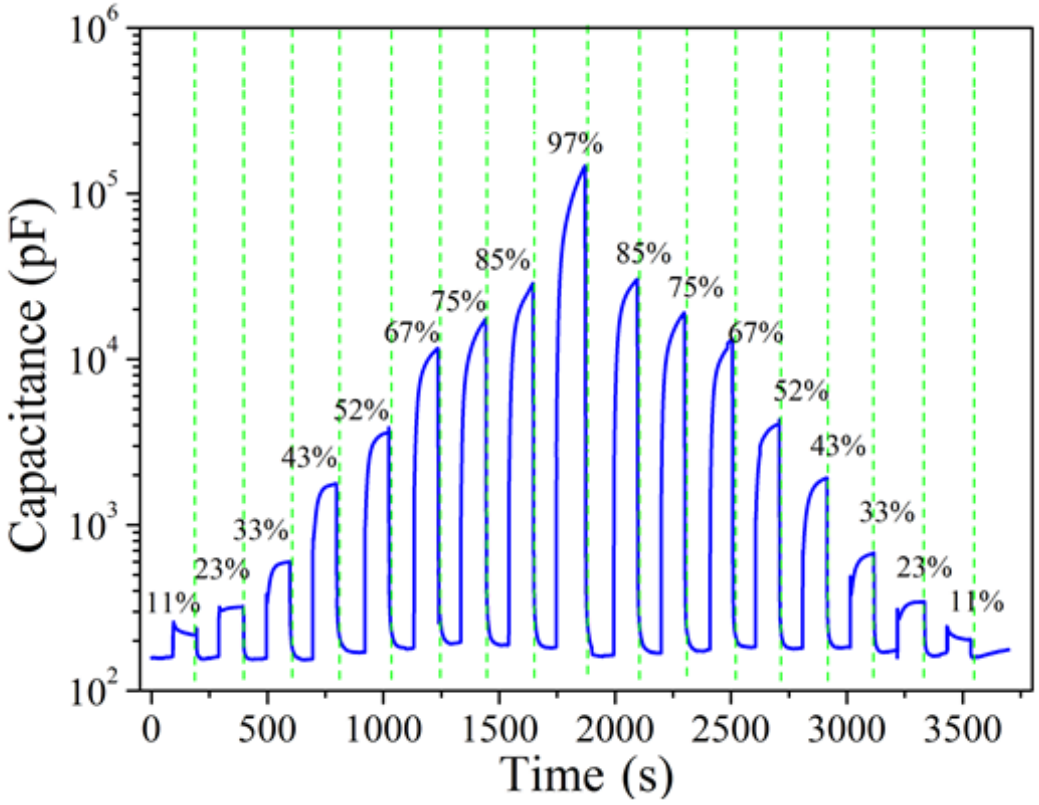


**Figure 5.** Capacitance response of the $SnO_2$/RGO hybrid composite sensor under switching RH.



Page 31 of 39

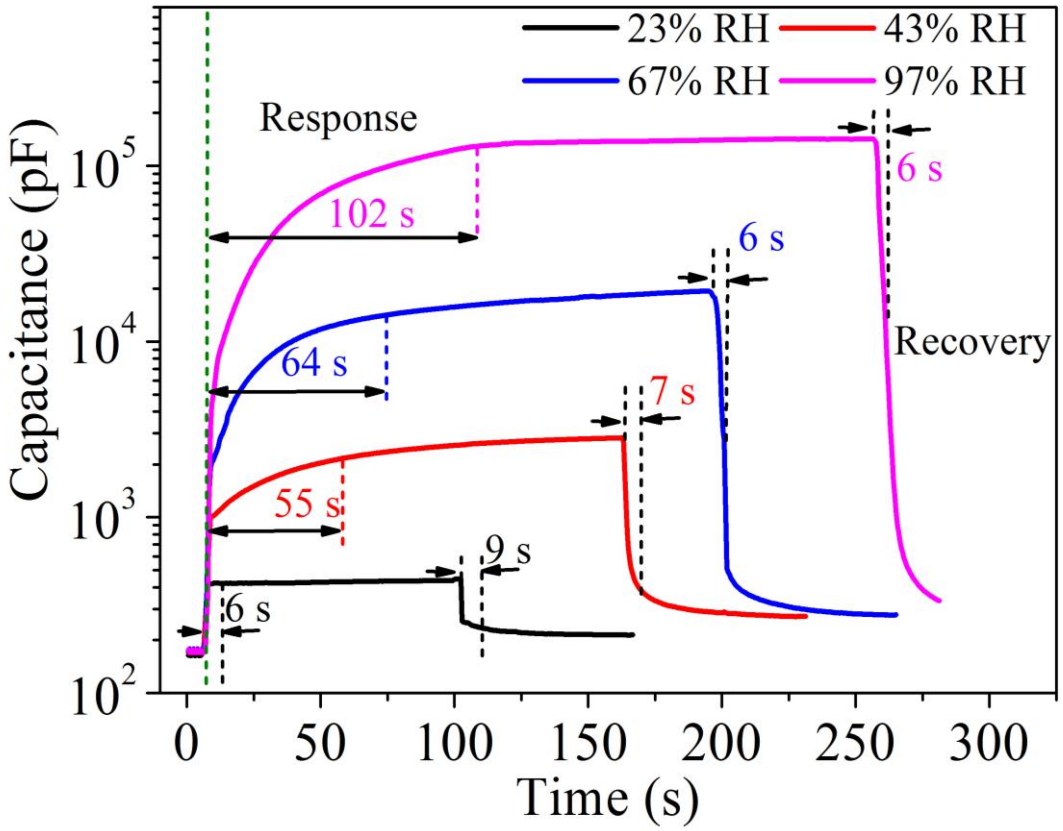


**Figure 6.** Response and recovery curves of the $SnO_2$/RGO hybrid composite sensor toward a RH pulse from dry air to other RH levels.



Page 32 of 39

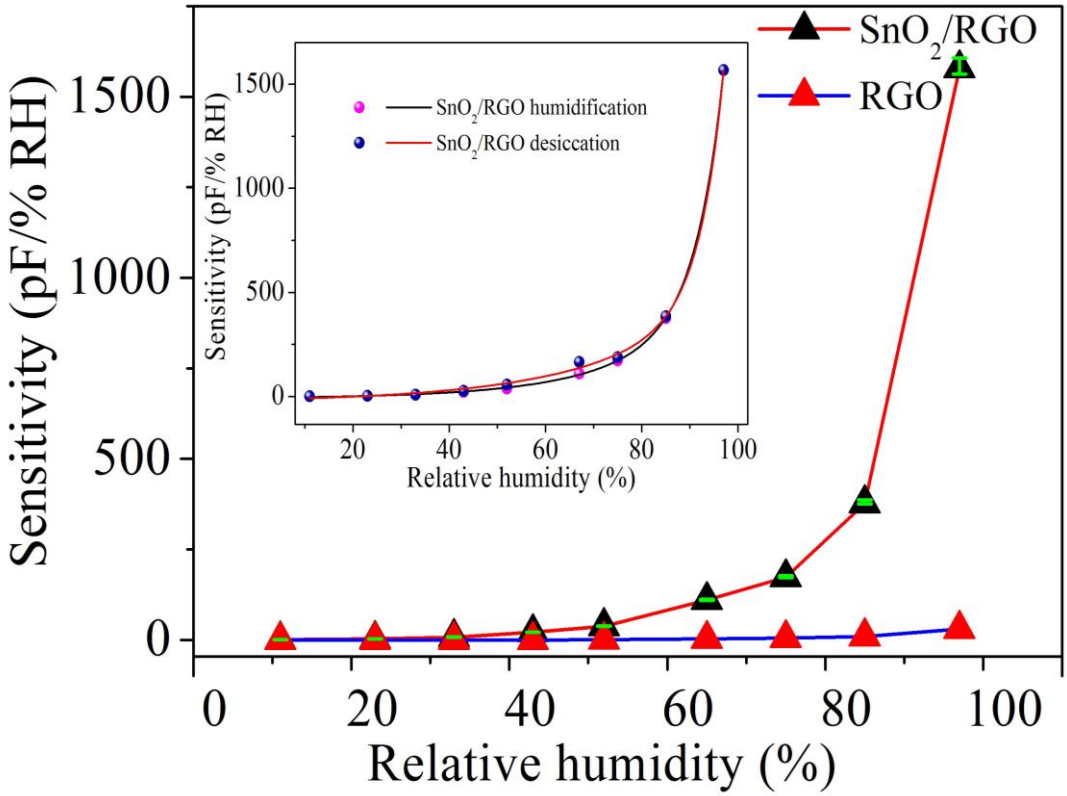


**Figure 7.** Sensitivity comparison between $SnO_2$/RGO composite and RGO toward humidity sensing. Inset: Hysteresis characteristic of the $SnO_2$/RGO composite humidity sensor.





Page 33 of 39

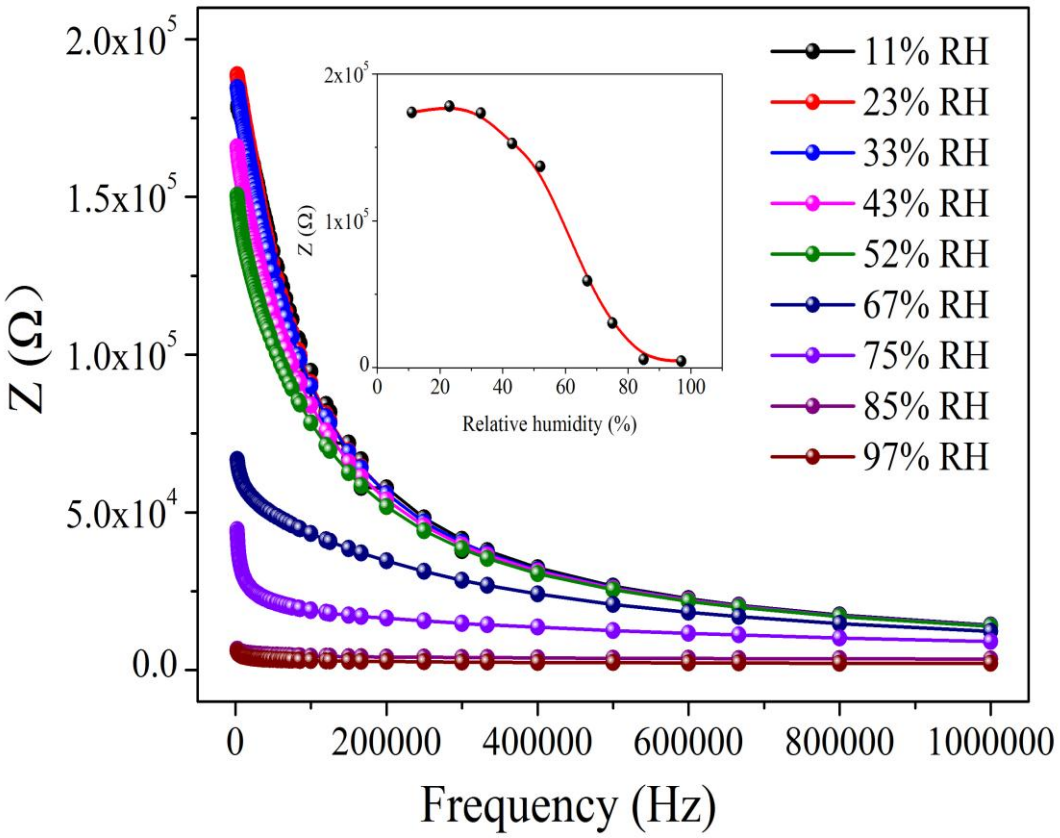


**Figure 8.** Impedance-frequency characteristics of the $SnO_2$/RGO hybrid composite sensor at various RH levels, the inset indicates the sensor impedance under various RH levels at 10 kHz.





Page 34 of 39

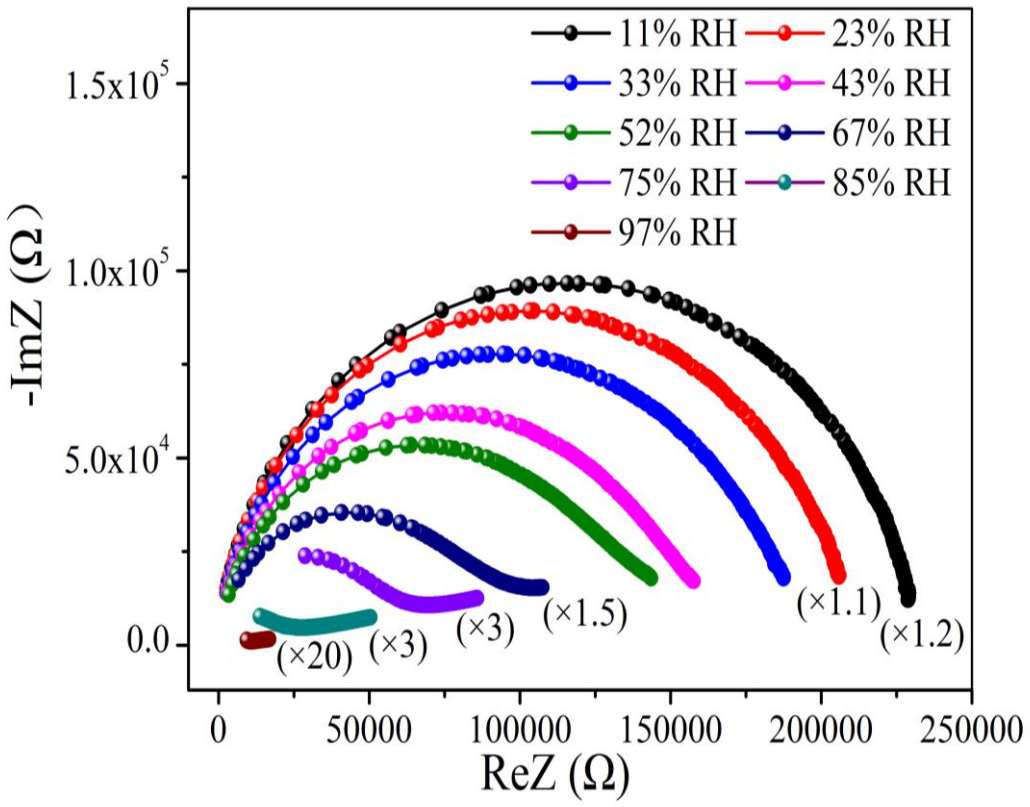


**Figure 9.** Complex impedance spectra of $SnO_2$/RGO film sensor at different relative humidity. ImZ: imaginary part; ReZ: real part.





Page 35 of 39

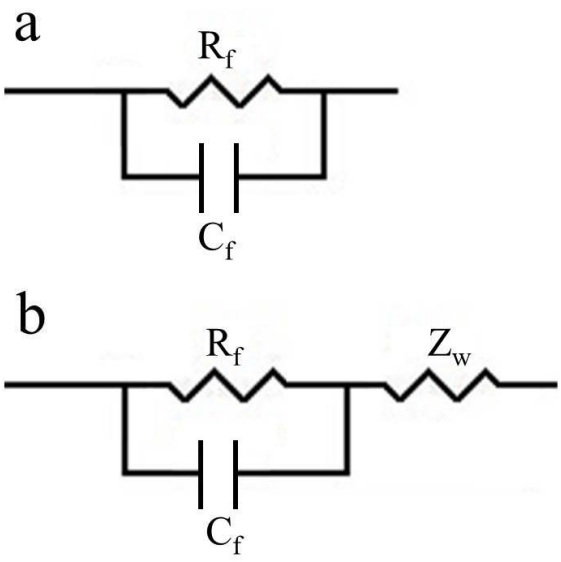


**Figure 10.** Impedance-frequency characteristics of the $SnO_2$/RGO hybrid composite sensor at different RH levels. $R_f$: film resistance; $C_f$: film capacitance; $Z_W$: Warburg impedance.

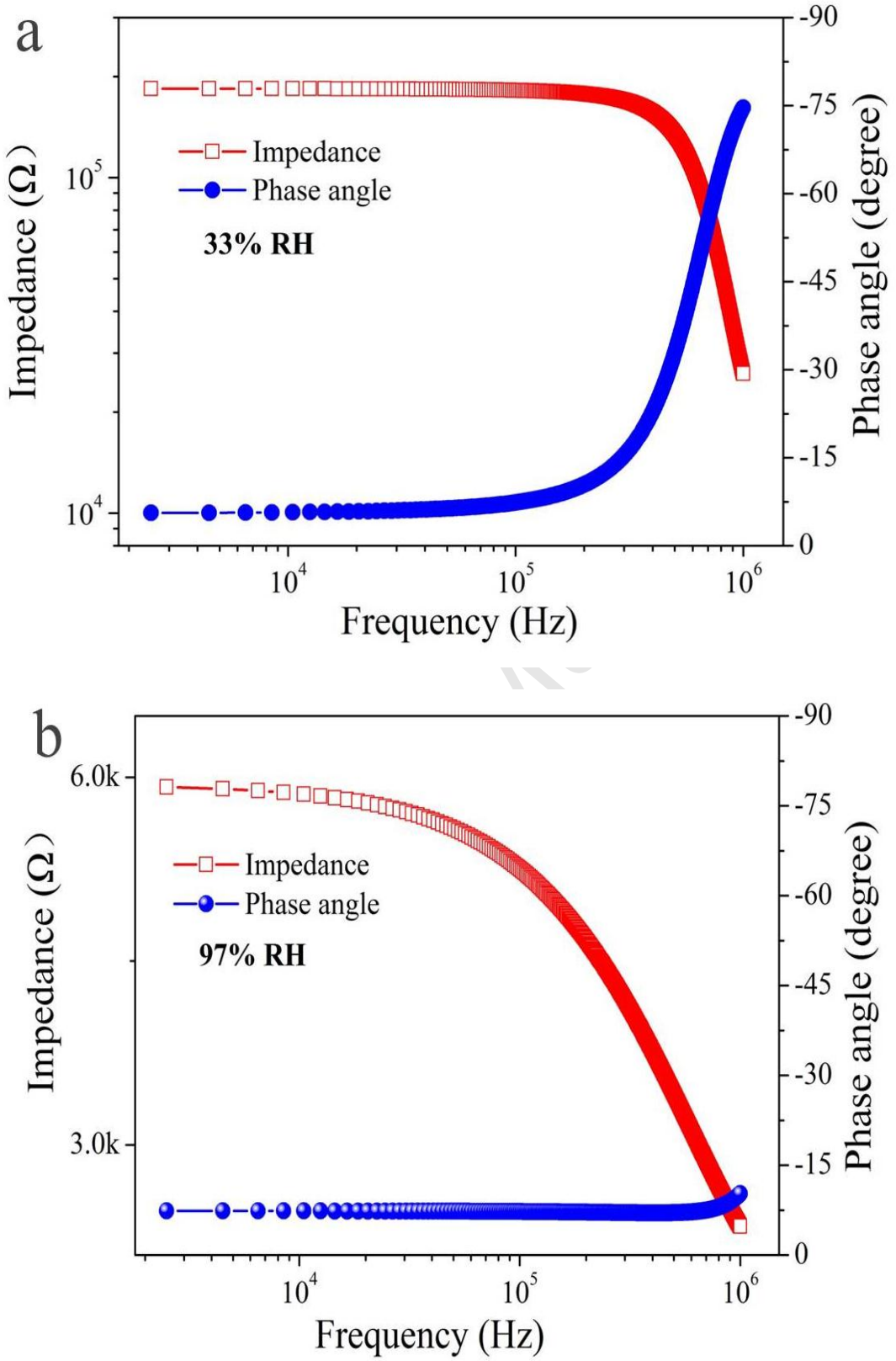


**Figure 11.** Bode diagrams of $SnO_2$/RGO hybrid composite sensor at different RH: (a) 33%RH, (b) 97%RH.

## Biographies

**Dongzhi Zhang** received his B.S. degree from Shandong University of Technology in 2004, M.S. degree from China University of Petroleum in 2007, and obtained Ph.D. degree from South China University of Technology in 2011. From 2009 to 2011, he worked as a visiting scholar of Mechanical Engineering at the University of Minnesota, U.S.A. He is currently an associate professor at China University of Petroleum (East China), Qingdao, China. His fields of interests are gas and humidity sensing materials, nanotechnology, and polymer electronics.

**Hongyan Chang** received her B.S. degree from Shandong University of Technology in 2012. Currently, she is graduate student at China University of Petroleum (East China), Qingdao, China. Her fields of interests include carbon nanomaterials-based gas sensors, electrical engineering and precision measurement technology.

**Peng Li** received B.S. degree in Electronic Engineering from Tianjin University, China, in 2007, and Ph. D. degree in Precision Instruments from Tsinghua University, China, in 2012. He is currently working in Department of Mechanical engineering at Tsinghua University. His current research interests include graphene material synthesis, and graphene NEMS device fabrication and their application in actuators and sensors.

**Runhua Liu** received his B.S. degree from China University of Petroleum in 1982, M.S. degree from University of Chongqing in 1988. Currently, he is professor at China University of Petroleum (East China), Qingdao, China. His main areas of interest are electrical engineering and precision measurement technology.

**Qingzhong Xue** received his Ph.D. degree in materials science and engineering from Tsinghua University in 2005. He is currently a professor at China University of Petroleum (East China). His research interest includes the fabrication and characterization of film materials, carbon nanotube/graphene-polymer composites, as well as to exploit their potential applications.